文章编号：1007-3124(2003)04-0071-08

Visualizations of horseshoe vortex structure

CHEN Jun
(State Key Laboratory for Turbulence and Complex Systems, Peking University, Beijing 100871, China)

Abstract: A visualization study of the instantaneous flow patterns in a laminar junction flow is presented in the paper. The pulsed hydrogen bubble technique and video recording system allows the recording of instantaneous flow field in the present study. The arrangement of the hydrogen bubble wire was proven to be critical for revealing the fine structure of the junction flow. The junction flows produced by a rectangular block extending from the surface were tested with Reynolds number ranging from $Re_{\delta^*} = 2.74 \times 10^2$ to 3.19×10^2. The results illustrate the existence of primary horseshoe vortices and counter-rotating secondary vortices. Some new features, such as the behavior of the head portion of a primary HV in the formation region and its shoulders upstream of the block, were found in the visualization study.

Key words: junction flow; horseshoe vortex; streaks; boundary layer

马蹄涡结构的显示

陈 军
(北京大学湍流与复杂系统国家重点实验室，北京 100871)

摘要：对层流角区流动的动态流动模式进行了流动可视化实验研究。实验采用了脉冲氢泡发生器和录像系统对流场进行了显示和研究。通过实验发现，氢泡丝的布置是清晰显示角区流动的精细结构的重要因素。实验雷诺数范围为 $Re_{\delta^*} = 2.74 \times 10^2 \sim 3.19 \times 10^2$。该实验的角区流动由在平板表面的长方形突起物产生。实验结果显示了主马蹄涡和反向二次涡的流动结构和流动过程。实验还发现了一系列新的流动现象，如马蹄涡的头部形成区域的流动过程及其在柱体上游形成"肩膀"的现象等。

关键词：角区流动；马蹄涡；斑纹；边界层
中图分类号：O357.4⁺3；O357.1　　**文献标识码**：A

0 Introduction

When the boundary layer flow encounters a bluff body extending from a surface, owing to the adverse pressure gradient created by the presence of the bluff body, a complex, three-dimensional flow develops in the junction region, forming a region of separation upstream of the bluff body. The impinging boundary layer develops into span-wise vortex structures, fed by the vorticity created upstream at the leading edge of the bluff body. The body also generates span-wise pressure gradient, causing the vortices legs to divert symmetrically, thus introducing a highly three-dimensional vortex system around the body. One or more vortices extending down stream on either side of the bluff body have been named as necklace or horseshoe vortices (HVs).

Junction flows occur in many practical applications, such as at a wing-body junction of the aircraft, turbine blade-hub junctions of the turbine engine, and in the cool-

* Received date: 2002-11-18
Biography: CHEN Jun(1968-), 男，牡丹江市人，高级工程师. 研究方向：实验流体力学.

ing flow past computer chips on a circuit board. For example, when a river flow encounters a bridge pier, the horseshoe vortices formed around the base of the pier scour the riverbed, and possibly remove rock and soil. These flows may weaken bridge foundations and cause the collapse of bridges (Holnbeck, et al. 1993).

Some physical factors that may influence the structures and stability of the HV have been studied. The quality of upcoming flow and the characteristic dimensions of the body determine the horseshoe-vortex system. The approach boundary layer displacement thickness Reynolds number $Re_{\delta}*$, is an important dimensionless parameter, which affects the characteristics of the laminar junction flow. The shape of the bluff body influences the horseshoe structures critically. To a first approximation, the pressure gradients around a body are determined by the shape of the body, say bluntness factor (Metha, 1984), the ratio of chord to thickness – C/T, the ratio of height to thickness – H/T, etc., and other factors, like the size of the body, the blockage of the flow channel, and the influence of other nearby obstacles.

Agui and Andreopoulos (1992) examined the flows around an upright wall-mounted circular cylinder, by means of visualization techniques using smoke and surface-oil, and time resolved measurements of the wall pressure, for two Reynolds numbers of $Re_D = 1.0 \times 10^5$ and 2.2×10^5, respectively. They concluded that the PHV is "wandering" in space with the amplitude of order one boundary layer thickness. The motion seems to be coupled with the arrival of the large-scale structures of the incoming boundary layer of the primary vortex. From smoke visualizations, large scale structures are found to be considerably stretched because the part nearest the wall is substantially decelerated while the outer part convecting downstream with unchanged velocity. They proposed that the flow in the junction region consists of several large-scale structures that form a new structure, the primary vortex. Strong eruption of wall fluid away from the wall was observed upstream of the primary vortex. This led to the formation of either a counter rotating vortex or a mushroom vortex. The authors also proposed that the primary vortex consists of several large-scale structures which originated in the oncoming boundary layer and acquired substantial additional vorticity.

Seal (1997) investigated the laminar vortex system at the junction of a surface mounted rectangular block, using PIV, at Reynolds number $Re_w = 3 \times 10^4$ and $Re_{\delta^*} = 2.98 \times 10^2$. He found that while the primary vortex strengthens and convects downstream, it also interact with the surface, generating opposite-sign vorticity via a local vortex induced pressure gradient effect (Doligalski et al., 1994). The vortex manifests itself as a region both under the vortex and as a growing tongue trailing the vortex. The eruption tongue severs the primary vortex from the impinging boundary layer vorticity, allowing the primary vortex to breakaway from the formation region. The vorticity comprising the vortex could cross diffuse with the corresponding opposite-sign vorticity generated at the surface and circulates around the vortex. As a result of the cross diffusion, the circulation of the primary vortex substantially decreases when it convects downstream toward the block. They proposed that the instability in the impinging shear layer formed by attachment of the impinging boundary layer is the mechanism for frequency selection of the periodic breakaway behavior.

Seal (1999) studied the vortex-vortex and vortex-surface interactions in the junction region of a circular cylinder mounted on a flat plate during the investigation of the HV controlled by suction of the flow upstream of a cylinder. The experiment was conducted at Reynolds numbers $Re_W = 7.8 \times 10^4$, and $Re_{\delta^*} = 4.81 \times 10^2$. Eruption process generated by the interaction of the intertwined vortices with the plate surface was found in the study. It was observed in the experiment that three-dimensional interactions of the braided vortices induce a pair of local surface-fluid eruptions reminiscent of the near-wall bursting that is characteristic of the near wall regeneration process for fully turbulent boundary layers. The authors suggested a new way to study the regeneration process – "burst" behavior in the near wall region by studying the HV interaction and associated vortex-surface interactions.

1 Apparatus

1.1 Water channel

Experiments were performed in a plexiglas free-surface water channel with a test section 0.3m deep × 0.3m wide

× 1m long. A rectangular bluff body was mounted on a 1meter long, 12mm thick, flat plexiglas plate with an elliptical leading edge. The water depth above the plate was 165mm. The free stream velocity U_∞ ranged from 40 ~ 65mm/s.

1.2 Visualization System

The power source for the hydrogen bubble generator consists of an autotransformer, which ranges between AC 0 ~ 270 volts, and a binode bridge generating direct current (DC). The pulse generator is a periodical switch circuit, which consists of an oscillation circuit, a frequency dividing circuit and a threshold circuit. This pulse generator has four different frequencies: 2, 4, 8 and 16 Hz. The switch-on time can be changed from full-"off" to full-"on". The control circuit is isolated from the power system by a relay. The generator is also integrated with an electrode reverse circuit for cleaning up the hydrogen bubble wire (Smith, et al., 2000).

A hydrogen bubble wire was used to visualize the junction flows and the structures in the boundary layer. Two types of hydrogen bubble wire arrangements are applied in the present research: namely the normal wire and the transverse wire.

For the normal wire system, the platinum wire was perpendicularly placed 400mm upstream of the leading edge of the plate, in the symmetric plane of the junction. The wire penetrated the plate and was fixed on the other side of the plate. The diameter of the hole is 1mm, carefully sealed and smoothed out with Blu Tack and thin tape. The other end of the wire was connected to the cathode of the hydrogen bubble generator, and was tensioned by a weight. The flat plate was placed horizontally, parallel to the bottom of the water tunnel.

For the transverse wire system, the hydrogen bubble wire was placed parallel to the plate wall, perpendicular to the mean flow, 3mm away from the wall, and 400mm upstream of the leading edge of the plate. The wire was fixed to two 3mm thick blocks, which were mounted on the edges of the plate. One end of the wire was fixed, and the other end was tensioned by a weight, and connected to the cathode of the hydrogen bubble generator. The plate was placed vertically in this wire set-up, so that no more adjustment for the lighting and camera system was necessary for shifting between the normal wire and the transverse wire.

The hydrogen bubble time-line was illuminated by a light source, located above the water channel. A light sheet was set up when the light passes through a slit covering the top of the channel. The thickness of the light sheet and a suitable brightness could be achieved by adjusting the width of the slit. The bubbles were lit by a 500w high-intensity photographic lamp.

The illuminated flows were recorded by a CCD camera and a Video Cassette Recorder, Mitsubishi HS-MX20V. The still pictures were captured by a workstation, Silicon Graphics, O_2. The image capture software is Media Recorder.

1.3 Model

The model was a rectangular block with the height of 155mm, the depth, 32mm, and the width, 64mm. The block was covered with black smooth tape to minimize light reflection. The block was normally mounted on the flat plate, 450mm from the leading edge.

2 Experimental results and discussions

2.1 Normal wire test

In this test, model-B of 64mm wide × 32mm deep × 155mm high was mounted on the flat plate. The hydrogen bubble wire was placed normal to the coming flow and the wall. In the test, the flow velocity was set $U_\infty = 54$mm, yielding the corresponding Reynolds number based on displacement thickness $Re_{\delta *} = 2.74 \times 10^2$ and Reynolds number based on the width of the block $Re_w = 3.6 \times 10^3$. According to the visualized results, the flow was in the amalgamating regime.

2.1.1 Topology

The junction flow is characterized by three unsteady primary horseshoe vortices. The vortices interact with each other in a quasi-periodic way, and some special phenomena occur intermittently.

Figure 1 shows a time sequence of the normal wire test. The frequency of the time line of the hydrogen bubble is $f_H = 4$Hz. The eruption and roll-up are visualized in figure 1(a) ~ (c). A thin plume of high levels of vorticity is

ejected upstream near the wall (see figure 1(a)). As the plume lifts up away from the surface, a deflection in the downstream direction is expected with an ultimate roll-up into a primary vortex. The impinging boundary layer vorticity is organized into a vortex. V-1 strengthens and advects downstream, assimilating more impinging boundary layer vorticity. Simultaneously, V-2 begins to interact with the plate surface, generating opposite-sign voritcity through a local vortex-induced pressure gradient effect that manifests itself as a region both directly beneath the vortex and as a growing tongue penetrating into the boundary layer when the vortex grows.

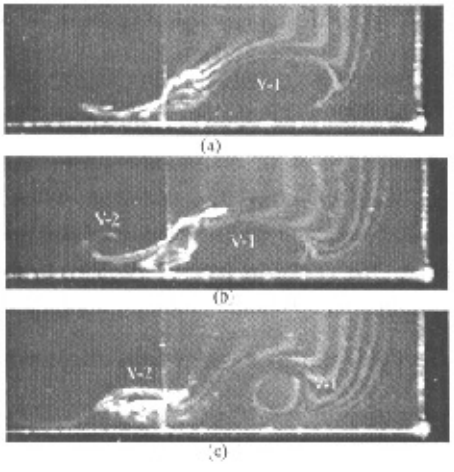

Fig.1 Time sequence of the junction flow upstream of model-B, the normal wire $f_H = 4Hz$

图1 模型B角区流上游的时序结构

Note that upstream of the eruption, some marking particles (hydrogen bubbles) still convect upstream, which infers that the front of junction flow region is not a half saddle but a half node on the plate. This agrees with the topology, which Visbal (1991) proposed in his study, shown in figure 2(a). Other visualizations reveal that the attachment line as the foremost line upstream of the primary horseshoe vortices is one of the common characteristics of junction flows at lower Reynolds number.

2.1.2 Mushroom-shaped vortex structure

Figure 3 presents a time sequence of the formation/break-up of a mushroom-like vortex pair. A mushroom-shaped vortex pair is expected to form at some instant when vorticity is concentrated in a strong vortex farther from the wall than usual. In the case of the present study, the core of the vortex distance from the wall is $Y/W = 0.26$, larger than usual primary convecting vortices, approximately $Y/W = 0.2$.

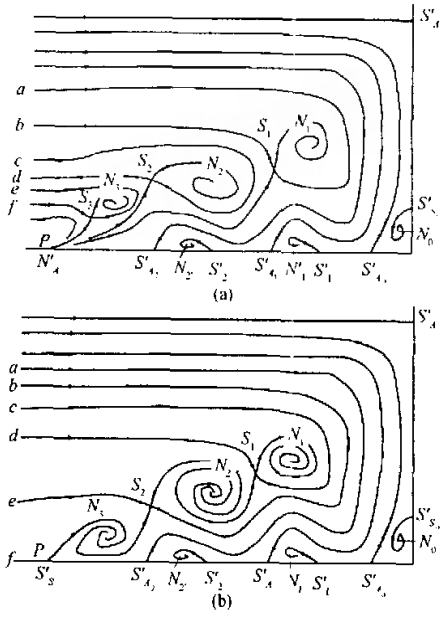

Fig.2 Two types of topology of laminar junction flow (Visbal.1991)

图2 角区层流的两类拓扑结构

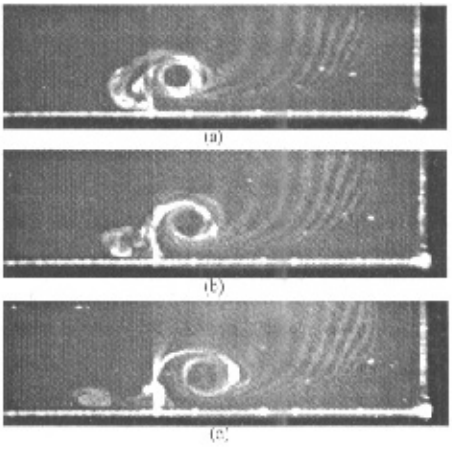

Fig.3 Time sequence of the mushroom-shaped vortex pair upstream of model-B, the normal wire $f_H = 4Hz$

图3 模型B上游蘑菇状涡对的时序结构

The topology is shown in figure 4. Note that as the counter-rotating vortex convects upstream away from the primary vortex, a saddle point evolves into two half-saddle points, which connect to each vortex. While this pair of

vortices separates gradually, the primary vortex moves downstream and the counter-rotating one convects upstream. During their convection the strength and the size of the primary vortex almost do not change, but the strength of the counter-rotating vortex decreases dramatically. Most vorticity in the counter-rotating vortex is consumed by the local high-speed downstream fluid, and dissipates upstream of the primary vortex.

2.1.3 Three-primary-vortex system

In the case of the normal wire test, the nature of the junction flow was characterized by a two-vortex and three-vortex hybridized unsteady flow. The two-vortex pattern and the three-vortex pattern appear in an intermittent way. The Reynolds-number-determined flow was in the regime between the two-vortex and the three-vortex flow pattern, hence the flow features were sensible to the coming flow conditions, and a variety of complex phenomena were observed in this regime. Three primary and two counter-rotating vortices are presented in Figure 5(a). The flow pattern is similar to Visbal's topology, shown in Figure 2(b). Note that no corner vortex was ovserved in all the flow conditions in the present study.

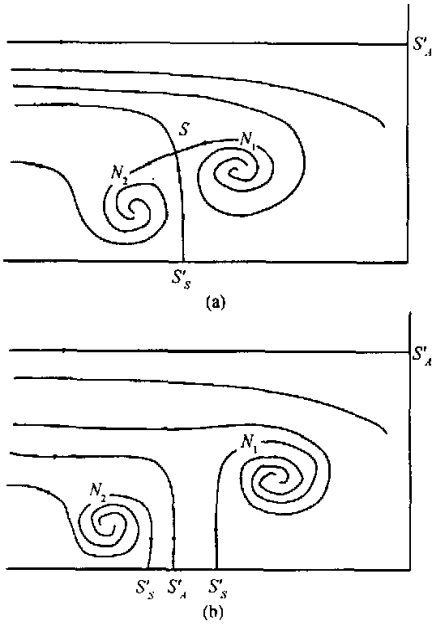

Fig.4 The topology mushroom-shaped vortex pair upstream of model-B

图 4　模型 B 上游蘑菇状涡对的拓扑结构

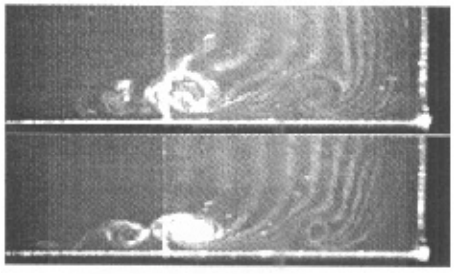

Fig.5 Visualization of typical three-primary-vortex structure upstream of model-B, the normal wire, $f_H = 4$Hz

图 5　模型 B 上游的三种典型涡的显示

2.2 Transverse wire test

The boundary-layer displacement thickness Reynolds number increases from $Re_{\delta^*} = 2.74 \times 10^2$, corresponding to the normal wire, to $Re_{\delta^*} = 3.06 \times 10^2$, corresponding to the transverse wire, and the nature of the flow changes from one pattern to another. The free stream velocity in this test is $U_\infty = 68$mm/s, which yielded $Re_L = 3.17 \times 10^4$ and $Re_W = 4.54 \times 10^3$, based on the width of the model w = 64mm respectively. According to the visualized results, the flow is in the breakaway regime.

2.2.1 The breakaway regime

Figure 6(a) ~ (g) show a time sequence of the vortex shedding process covering one complete vortex generation breakaway circle when V-0 (Vortex 0) is about to dissipate because of stretching, and V-1 (Vortex 1) is convecting toward the block (figure 6(a), $T = 0$s). Note that while V-1 is approaching the block, V-2 at the sides of the block begins to convect with the high free flow stress around the block. The "shoulders" of V-2 appear and curve toward

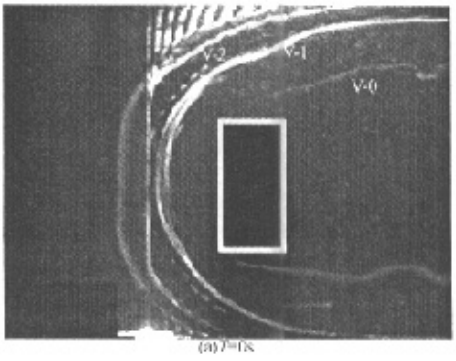

(a) $T=0$s

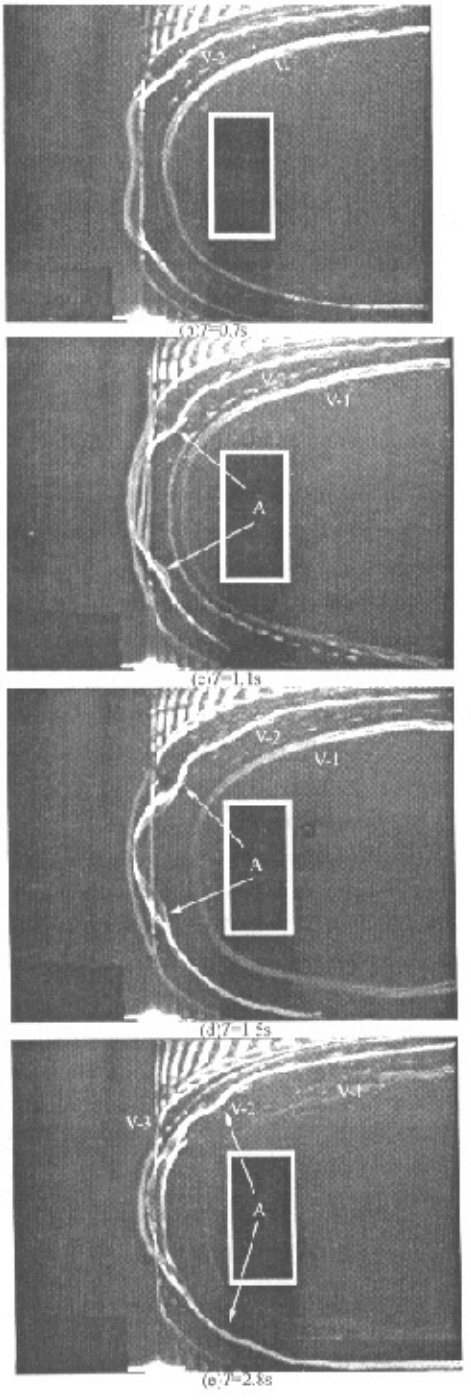

Fig.6 ***A time sequence of the transverse wire visualisation of model-B. "A" indicates the shoulders of the vortex; "B" indicates the boundary of the new vortex.***

图 6 模型 B 横向剖面显示的时序结构，A 代表涡"肩部"B 代表新涡的边界

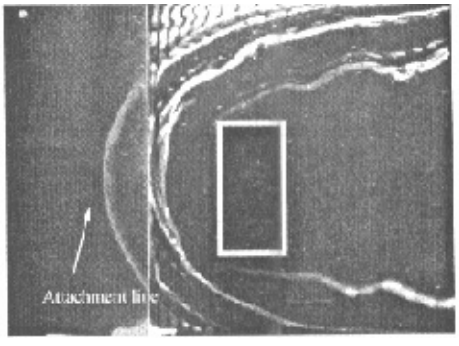

Fig.7 The attachment line of junction flow Model-B, The transverse wire $f_H = 8Hz$

图 7 模型 B 角区流动的附着线

the block, by "A" (figure 6(c) $T = 1.1s$).

The vorticity is concentrated in V-2 legs at first, and then in the head of the vortex. The strong backward flow sweeps the hydrogen bubbles upstream quickly (figure 6 (c), $T = 1.1s$). The shoulders of V-2 continue moving inwards. The upstream-sweeping bubbles decelerate upstream of the block, forming a foremost line - the coalescence line (figure 7 and figure 6(d), $T = 1.5s$). Then a

whole new HV forms. The vortex tube can be clearly visualized with hydrogen bubbles around the wire. The shoulders of the newly formed vortex move downstream along the vortex legs (figure 6(e), $T = 2.8$s). A new vortex is developing at the outermost side of the horseshoe vortices, indicated by "B" in figure 6(f)-(g), and it finally sheds from the boundary layer (figure 6(g), $T = 3.2$s).

2.2.2 The topology of the junction flow

The topology of the horseshoe vortices is studied in this case. The visualisation results are in accordance with the new type of laminar HV topology (Visbal, 1991). In other words, the foremost line of coalescence is an attachment rather than a separation line, namely the jet-maze topology. Figure 7 shows an instant when the bubbles reach the foremost line of coalescence. When the newly formed horseshoe vortex – V-2 is passing the wire and convecting toward the block, some reverse sweeping bubbles reach the foremost line, as shown in figure 7 and 6(f). This proves that the foremost line is an attachment line, rather than a separation line. If this foremost line is a separation line, all bubbles there should be entrained by the newly formed horseshoe vortex – V-2, when it convects toward the block, rather than some of them forming a hydrogen-bubble-material line moving upstream.

In fact, this topology is difficult to visualize by ordinary means, like dye injection or a hydrogen bubble wire. Taking the normal wire for instance, because of the periodic shedding process, it is hard to detect the saddle point upstream of the new horseshoe vortex. Moreover, since streamlines are velocity dependent (Perry & Chong, 1987), the critical points in the flow are not easily observed from visualizations.

2.2.3 The structure of HV

A schematic diagram of the HV tubes is shown in figure 8, corresponding to the time $T = 3.0$s (figure 6(f)). Note that at the moment when V-3 (Vortex 3) still has not formed a visible vortex section in the symmetry plane, the vortex legs of V-3 has distinctively developed at the sides of the block (see figure 6(g), indicated by "B"). It is different from the common picture described by some previous observations. This contradicts most previous studies, which suggest that the formation of every portion of a HV is completed simultaneously, from the head to the legs. The reason for these contradictory observations may be caused by different visualisation techniques.

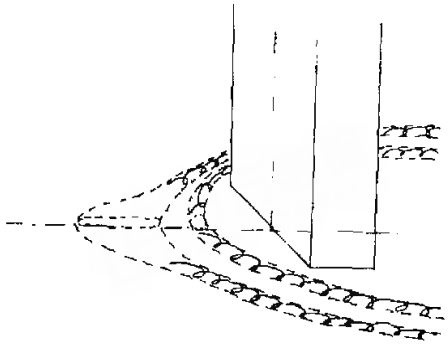

Fig.8 The schematic diagram of the breakaway of the horseshoe vortex

图 8　马蹄涡分离的示意图

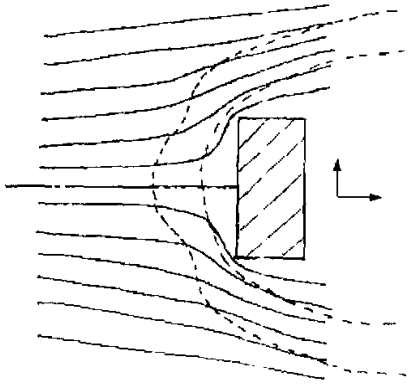

Fig.9 The schematic diagram of the relationship between primary horseshoe vortices and the streamlines above them. Dash lines stand for primary HV; solid lines stand for streamlines

图 9　基本马蹄涡和绕流线之间关系的示意图.虚线:马蹄涡,实线:流线

The present analysis shows that the formation of the initial vortex – V-3, (as shown in figure 6(e) ~ (g)) is developed in a region near the wall. The size of the V-3 at the very first moment when it forms is of the order of the distance between the transverse wire and the wall – $O(\delta^*)$. Such a vortical filament formed near the surface is very difficult to demonstrate if the marking particles are far from the wall. It is reasonable to question the general picture of the HV shedding process presented by the transverse wire far from the wall, compared with results shown by the transverse wire set-up in the approach boundary layer. In

other words, conventional visualizations seem only present in the later process after the new vortex has already broken away.

2.2.4 The shoulders of the new HV

The local rising of the vortex accounts for the formation of shoulders (indicated by "A" in figure 6(c) ~ (e)), during the head of the vortex convecting toward the block. From the streamlines upstream of the junction, as shown in figure 9, it is seen that the flow is accelerated when passing the region near the upstream corners of the block, and the vortex is compressed in this region. The vortex under the flow rises up and is entrained by the fast flow convecting downstream, faster than other portions of the vortex. As a result, this portion of the vortex line curves downstream.

3 Conclusion

(1) Visualizations of the flow field reveal that the attachment line as the foremost line upstream of the primary horseshoe vortices is one of the common characteristics of junction flows at lower Reynolds number. In other words, there is a half node rather than a half saddle on the symmetric plate. This agrees with the topology, which Visbal (1991) proposed in his study, shown in figure 2(a).

(2) A time sequence of the formation/break-up of a mushroom-like vortex pair was clearly revealed. A mushroom-shaped vortex pair is expected to form at some instant when vorticity is concentrated in a strong vortex farther from the wall than usual.

(3) The shoulders of the newly created HV were observed in the present study. This observation implied that the head of the HV is not necessarily to be a U-shaped vortex tube during its formation. The observation suggests that the formation of the primary horseshoe vortices begins from the legs rather than starting simultaneously along the whole primary HV.

(4) The position of the hydrogen bubble wire is critical for the visualisation quality. The fine structures and flow patterns have to be revealed by more reasonable arrangement of the particle release position. Moreover, the hydrogen bubble wire should be placed near the wall if the cause of the HV is the aim of the experimental research.

References:

[1] AGJI J H, ANDREOPOULOS J. Experimental investigation of a three-dimensional boundary layer flow in the vicinity of an upright wall mounted cylinder. Trans. ASME. 1992,114, 566 ~ 576.

[2] DOLIGALSKI T L, SMITH C R, WALKER J D A. Vortex interactions with walls. Ann. Rev. Fluid Mech.,1994, 26, 573 ~ 616.

[3] HOLNBECK S R, PARRETT C, TILLINGER T N. Bridge scour and change in contracted section. Razor Creek, Montana, Hydraulic Engineering, 1993,2, 2249 ~ 2254.

[4] METHA R D. Effect on a wing nose shape of the flow in a wing/body junction. Aerosp. J.1984, 88, 456 ~ 60.

[5] PERRY A E, CHONG M S. A description of eddying motions and flow patterns using critical-point concepts. Ann. Rev. Fluid Mech. 1987,232, 99 ~ 131.

[6] SEAL C V, SMITH C R, WALKER J D A. Dynamics of the vorticity distribution in end wall junctions. AIAA 1997, 35, 1041 ~ 47.

[7] SEAL C V, SMITH C R. Visualization of a mechanism for three-dimensional interaction and near-wall eruption. J. Fluid Mech. 1999,394, 193 ~ 203.

[8] SMITH C R, SEAL C V, PRAISNER T J, SABATINO D R. In flow visualization techniques and examples. Imperial College, 2000,27 ~ 42.

[9] VISBAL M R, Structure of laminar juncture flows. AIAA J. 1991,29(8): 1273 ~ 1282.